Biomaterials Science

ROYAL SOCIETY OF CHEMISTRY

PAPER

View Article Online
View Journal | View Issue

Cite this: *Biomater. Sci.*, 2023, **11**, 7926

Collagen biomaterials promote the regenerative repair of abdominal wall defects in Bama miniature pigs

Langfan Qu,†[a] Zelin Chen,†[a] Jianhua Chen,†[b,c] Yibo Gan,[d] Xu Tan,[a] Yu Wang,[a] Can Zhang,[a] Bing Chen,[e] Jianwu Dai,*[e] Jianxin Chen*[b] and Chunmeng Shi *[a]

Due to adhesion and rejection of recent traditional materials, it is still challenging to promote the regenerative repair of abdominal wall defects caused by different hernias or severe trauma. However, biomaterials with a high biocompatibility and low immunogenicity have exhibited great potential in the regeneration of abdominal muscle tissue. Previously, we have designed a biological collagen scaffold material combined with growth factor, which enables a fusion protein-collagen binding domain (CBD)-basic fibroblast growth factor (bFGF) to bind and release specifically. Though experiments in rodent animals have indicated the regeneration function of CBD-bFGF modified biological collagen scaffolds, its translational properties in large animals or humans are still in need of solid evidence. In this study, the abdominal wall defect model of Bama miniature pigs was established by artificial operations, and the defective abdominal wall was sealed with or without a polypropylene patch, and unmodified and CBD-bFGF modified biological collagen scaffolds. Results showed that a recurrent abdominal hernia was observed in the defect control group (without the use of mesh). Although the polypropylene patch can repair the abdominal wall defect, it also induced serious adhesion and inflammation. Meanwhile, both kinds of collagen biomaterials exhibited positive effects in repairing abdominal wall defects and reducing regional adhesion and inflammation. However, CBD-bFGF-modified collagen biomaterials failed to induce the regenerative repair reported in rat experiments. In addition, unmodified collagen biomaterials induced abdominal wall muscle regeneration rather than fibrotic repair. These results indicated that the unmodified collagen biomaterials are a better option among translational patches for the treatment of abdominal wall defects.

Received 21st July 2023,
Accepted 19th October 2023

DOI: 10.1039/d3bm01209c

rsc.li/biomaterials-science

1. Introduction

Muscle tissue, accounting for more than 50% of the body mass, plays a vital role in the human body by controlling the production of strength, the movement of the body and the function of the internal organs.[1–3] Muscle tissue can regenerate after minor injury.[4,5] This depends on muscle stem cells (MuSCs), also known as "satellite cells", and their interaction with the surrounding microenvironment.[5,6] However, this regenerative ability fails to exert due to trauma or surgical removal of a critical part of a muscle or muscle unit, a condition known as volumetric muscle loss (VML).[7] Therefore, there is an urgent need for a new and efficient regenerative strategy to reverse the situation.

The large and complex abdominal hernia model can be considered as an ideal model for VML.[8] At present, patch materials transplantation is the only clinical strategy for the treatment of abdominal hernia.[9] The traditional patch material, represented by polypropylene (PP), is inelastic, non-absorbable and plastic. More importantly, an immune rejection would also be induced by these traditional materials, manifested as chronic pain, foreign body sensation, adhesion, giant fibrous cyst formation, intestinal obstruction, *etc.*[10] Recently, tissue engineering has shown great potential in a range of regeneration medicine including muscle tissue engineering.[11] Muscle tissue engineering is a combination of biomaterials, cells and growth factors to form functional tissues, and

[a]*Institute of Rocket Force Medicine, State Key Laboratory of Trauma and Chemical Poisoning, Third Military Medical University, Chongqing 400038, China. E-mail: shicm@sina.com*
[b]*Key Laboratory of OptoElectronic Science and Technology for Medicine of Ministry of Education, Fujian Provincial Key Laboratory of Photonics Technology, Fujian Normal University, Fuzhou 350117, China. E-mail: chenjianxin@fjnu.edu.cn*
[c]*College of Life Science, Fujian Normal University, Fuzhou 350117, China*
[d]*Department of Spine Surgery, Center of Orthopedics, State Key Laboratory of Trauma and Chemical Poisoning, Daping Hospital, Army Medical University (Third Military Medical University), Chongqing 400042, China*
[e]*Institute of Genetics and Developmental Biology, Chinese Academy of Sciences, Beijing 100101, China. E-mail: jwdai@genetics.ac.cn*
†These authors contributed equally to this work.

is considered to be a promising treatment for muscle injury. Of note, biomaterials are the key factor of muscle tissue engineering as muscle regeneration may be triggered by them. Biomaterials have been shown to attract myeloid and lymphoid immune cells,[12–14] putative perivascular stem cells,[15,16] and fibroblasts (based on tissue deposition).[15,17–19] The recruitment of myriad cell populations and their activity is proposed to occur in a spatiotemporal sequence that culminates in the regeneration of a volume of muscle tissue that may impart functional improvements.[20] Processing of biological scaffolds, as well as the initial tissue themselves, are heterogeneous and, therefore, different scaffolds may be presented with variable compositions and structures, which may impact the performance *in vivo*.[21] Therefore, developing biomaterials based on muscle tissue engineering is of great significance.

Collagen biomaterials possess the characteristics of low immunogenicity, good biocompatibility and biodegradability.[22,23] In addition, collagen biomaterials could send biological signals to the surrounding tissues to activate the intrinsic repair response. Basic fibroblast growth factor (bFGF) is a potent mitogen that plays an important role in a variety of pathophysiological processes. It regulates the growth, migration, differentiation, and survival of many cell types, including fibroblasts, vascular endothelial cells, and smooth muscle cells, and also impacts tissue remodelling, wound healing, and neovascularization.[24,25] In muscle injury repair, Kim *et al.* reported that bFGF could promote smooth muscle regeneration and exerted a good therapeutic effect against urinary incontinence.[26] Our previous studies have indicated that collagen biomaterials especially modified with human bFGF held the possibility to induce the regenerative repair of full-thickness abdominal wall defects in rats.[27] However, more evidence of the effects of the collagen biomaterials modified with human bFGF in large animal models is needed to promote clinical implementation.

Here, we established an abdominal wall defect model in Bama miniature pigs, and verified the repair effects of collagen materials with or without CBD-bFGF modification and traditional polypropylene materials. We hypothesized that all of the traditional patch and collagen biomaterials can repair the abdominal wall defect, however, recurrence of hernia, serious adhesion and inflammation might occur only in polypropylene; additionally, the regenerative repair could be induced by CBD-bFGF-modified collagen biomaterials while it could not be induced by unmodified ones.

2. Experimental

2.1 Preparation of biological collagen scaffold

The collagen membrane, purchased from Zhenghai Biotechnology Co., Ltd, was made of cowhide treated with a methanol : chloroform (1 : 1) solution and designed as a three-dimensional structure similar to natural collagen. Then, the unwanted tissues were washed off by ultrasound. In order to remove the cellular components, the sample was treated with 0.2% Triton. The freeze-dried membrane was then cut into 8 cm × 6 cm slices, sterilized by 12 kGy Co-60 irradiation before use, and sterilized by ethylene oxide.

The preparation of CBD-bFGF protein was in accordance with that in previous studies.[28,29] The CBD-bFGF gene containing a His6 tag was amplified by a polymerase chain reaction and cloned into vector pET-28a. The gene was transformed into *E. coli* BL21 (DE3) and induced by IPTG. The recombinant protein was purified by nickel column chromatography.

150 μg of bFGF was dissolved in 2 ml of aseptic phosphate buffered saline, then dropped into collagen scaffold, with a specified CBD-bFGF dosage of 64 μg g^{-1} collagen membrane weight, and was stored at 4 °C until implanted.

2.2 Observation of material structure by a scanning electron microscope

Polypropylene patches were purchased from Rizhao Tianyi Biomedical Technology Co., Ltd. Samples of the three materials were fixed overnight with 2.5% glutaraldehyde (Sigma), cleaned with 0.1 M sodium bicarbonate buffer for 3 × 15 min, fixed with 0.1% OsO_4 (Sigma) at room temperature for 2 h, washed with water for 2 × 10 min and dehydrated. Dehydration steps were: 35% ethanol 10 minutes, 50% ethanol 10 minutes, 70% ethanol 10 minutes, 90% ethanol 10 minutes, 2 × 100% ethanol 15 minutes. Isoamyl acetate was replaced for 2 × 15 min. After drying, gold was sprayed and the imaging was observed by an electron microscope.

2.3 Surgical procedure

All the animal experiments were approved by the Ethics Committee of the Third Military Medical University and carried out in accordance with the guidelines of the National Institutes of Health on the care and use of laboratory animals. 20 healthy female Bama miniature pigs, weighing 10–14 kg, were randomly divided into 5 groups: CBD-bFGF group, collagen group, polypropylene patch group, defect control group and Sham-operated group. Anaesthesia with ketamine (5 mg kg^{-1}) followed by intramuscular injection of diazepam (1 mg kg^{-1}) to maintain propofol 5–10 mg kg^{-1} h^{-1}. In addition to the sham operation, only incision and immediate suture of the skin, an aseptic surgical technique was used in all groups to construct a 4 × 4 cm abdominal wall defect on both sides of the groin in the preperitoneal space. Then, the patch was cut to 6 × 6 cm. Except for the defect control group, the abdominal hernia gap was sealed with a CBD-bFGF modified biological glue material, unmodified biological glue material and polypropylene membrane patch, respectively, and the abdominal hernia gap was sutured with a 6-0 suture (Fig. 1), and then the skin was sutured with a 3-0 thread in each group. Immediately after operation, they had free access to food and water, and penicillin (600 000 units) was injected intramuscularly once a day for 5 days. All the animals were sacrificed to acquire the samples, with no serious wound infection observed.

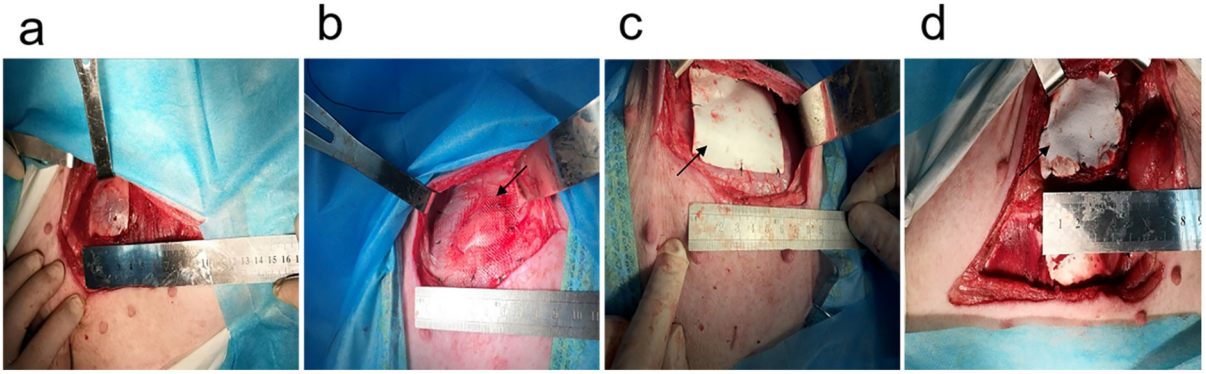

Fig. 1 Establishment of abdominal wall defect model in Bama miniature pigs. (a) Defect control group. (b) Polypropylene patch group. (c) Collagen group. (d) CBD-bFGF group.

2.4 Evaluation of recurrence and adhesion of abdominal hernia

The recurrence and adhesion of abdominal hernia were evaluated at 90 days and 180 days after operation. In the evaluation of the recurrence of abdominal hernia, the defect control group was used as the negative control group. The appearance of the abdominal wall of Bama miniature pigs was photographed in the standing state and in the anaesthetic decubitus position to observe the recurrence of abdominal hernia. Polypropylene membrane is widely used in clinical abdominal wall repair, but it easily causes serious infection and has a high incidence of adhesion.[30,31] Therefore, in terms of adhesion evaluation, using a polypropylene membrane as a negative control, animals were euthanized (excessive pentobarbital sodium; 90 mg kg^{-1}), and the abdomen was opened along the original incision without interfering with the adhesion, and photos were taken to record the degree of adhesion at the repaired site. The adhesion score was scored blindly by two independent observers. Grades ranged from 0 to 3, with 0 = no significant adhesions, 1 = thin, narrow, and easily detachable adhesions, 2 = thick adhesions limited to one area, and 3 = thick and broad adhesions involving the anterior or posterior abdominal wall and the viscera.[31,32]

2.5 Histologic analysis

Euthanasia was performed on the 90th and 180th day after operation (pentobarbital sodium overdose; 90 mg kg^{-1}). The long tissue bands of 4 cm, including the material, material-host tissue interface and adjacent host tissue, were removed from the abdominal wall of the implanted material. After 10% formalin fixation, 5 mm paraffin sections, haematoxylin-eosin staining and Masson staining were prepared and observed under a light microscope.

The muscle regeneration and inflammatory cell infiltration of different repair materials were analysed by immunohistochemical staining. Anti-α-smooth muscle actin antibody (α-SMA, 1 : 400, Abcam) and anti-CD163 antibody (1 : 100, ZSGB-Bio) were used to detect actin positive cells and inflammatory reaction. The samples were magnified and quantified by a double-blind method using IMAGE-Pro Plus software. Percentage of positive area = Positive area/Total tissue area.

2.6 Extraction of morphological and structural characteristics of collagen from repaired tissue by multiphoton microscopy

All regions of interest (ROI) were imaged by MPM (LSM 880 Zeiss, Germany) on the dewaxed sections of each sample. An excitation wavelength of 810 nm was selected for nonlinear optical imaging. A 32-channel GaAsP photomultiplier tube array detector was used to collect a two-photon excitation fluorescence (TPEF) signal in the wavelength range of 430–695 nm and a second harmonic generation (SHG) signal in the wavelength range of 395–415 nm. Subsequently, 5 visual fields of the sections within a field of view of 425.1 μm × 425.1 μm were selected to extract eight collagen morphological features by MATLAB 2016b (**https://github.com/qldqq1984/CollagenFeature**), namely, the collagen percentage area, fiber number, average fiber length, average fiber width, average fiber straightness, cross-link density, average cross-link space and orientation (Table 1).[33–36]

In terms of morphological features, a segmentation algorithm based on the Gaussian mixture model[33] was used to binarize the SHG image into collagen pixels and background pixels. Then, the fiber network extraction algorithm[34] was used to process the binary image and identify the skeleton of each collagen fiber. After fiber extraction, a list of ordered vertices[35] was established to calculate the 8 collagen morphological features. If any vertex in the list belonged to more than one fiber, it would be judged as a cross-linking point (connection points between collagen fibers). Finally, the arrangement of collagen was quantified by Fourier-transform analysis.[36]

2.7 Statistical analysis

Quantitative data were expressed as mean ± standard deviation (SD) and statistical analyses were performed by SPSS software (23.0). One-way ANOVA was used to compare data of multiple groups. All statistical tests were two-sided, and P values of less than 0.05 were deemed significant.

Table 1 Collagen morphological features

Feature	Description
Percentage area	The percentage of pixels in the segmented image
Fiber number	The number of collagen fibers extracted per square micron in the segmented image
Average fiber length	The mean length of the identified collagen fibers. The length of each fiber is defined as the sum of the distances between adjacent vertices
Average fiber width	The average distance between a vertex and its nearest background pixel
Average fiber straightness	The mean straightness of the identified collagen fibers. The straightness of each fiber is defined as the distance between the first and last vertices in the list divided by the fiber length
Fiber cross-link density	The ratio of the total number of cross-link points to the sum of lengths of all the collagen fibers in the segmented image
Average cross-link space	The average distance between adjacent cross-link points for each fiber in the segmented image
Orientation	The principal direction is determined according to the angular orientation distribution in the Fourier-transformed image

3. Results

3.1 Characterization of patch materials

Images of the scanning electron microscope (SEM) have shown that the collagen materials were a loose and porous structure with a pore size between 50 and 200 μm, which was significantly smaller than that of the polypropylene mesh (Fig. 2). This structure profited the diffusion of CBD-bFGF and further cell adhesion and crawling in tissues.

3.2 Collagen biomaterials presented a decreased recurrence and less adhesion of abdominal hernia

The recurrence of abdominal hernia was evaluated at 90 days after surgery. Photos of the abdominal hernia showed that CBD-bFGF modified collagen biomaterials, unmodified collagen biomaterials and polypropylene patches could effectively prevent recurrent abdominal hernia (Fig. 3a–d) 90 days after operation, while animals in the control group were observed with significant abdominal hernia. We further estimated the degree of adhesion of each experimental group. We found that the adhesion degrees in collagen with or without CBD-bFGF groups were significantly lower than that in the polypropylene patch group, displaying a better material fusion with the adjacent tissues. More specifically, the adhesion degree in collagen without CBD-bFGF groups was slightly lower than that in the CBD-bFGF groups, but there was no significant difference between the two groups (Fig. 3e–i). These results indicated that collagen biomaterials could prevent the recurrence of abdominal hernia as well as the traditional patches, but exhibiting less adhesion than the traditional material.

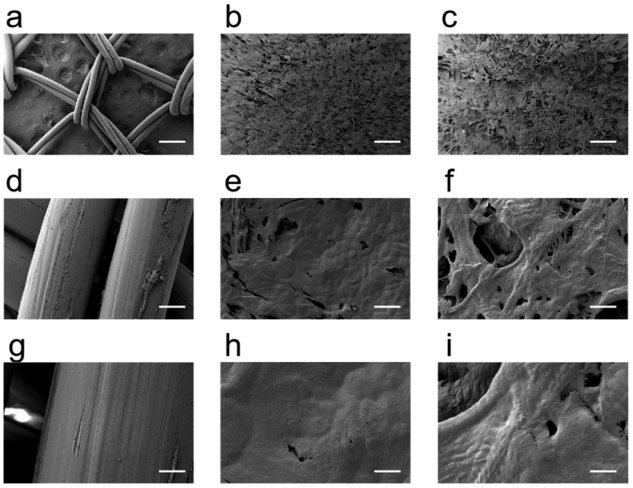

Fig. 2 Comparison of microstructure of different repair materials. (a, d and g) SEM images of polypropylene membrane. (b, e and h) SEM images of unmodified collagen biomaterials. (c, f and i) SEM images of CBD-bFGF collagen composite biomaterial. Scale bars, 500 μm (1st row) or 50 μm (2nd row) or 10 μm (3rd row).

3.3 Collagen biomaterials decrease inflammatory response and induce muscle regeneration

To further detect whether collagen biomaterials induce the regenerative repair of abdominal hernia, we harvested the wounded tissues at 90 d and 180 d after surgery. In normal conditions, the muscles of the abdominal wall were tightly and neatly arranged. However, HE staining showed that the abdominal wall was filled with a large amount of tight and thin extracellular matrix in the control group at 90 d and 180 d. And a tight and thick extracellular matrix was observed in the polypropylene patch group, with a relatively loose and thick extracellular matrix in the CBD-bFGF group. Interestingly, this showed significant muscle regeneration in the injured abdominal wall in the collagen group (Fig. 4a). The results of Masson staining further confirmed the extracellular matrix deposition in the control, polypropylene patch and CBD-bFGF groups, with muscle fiber regeneration in collagen group (Fig. 4b).

Collagen is one of the key microenvironments that induces the regenerative repair of the muscles. In order to further analyse the types of collagen during the regenerative repair in different groups, we performed Sirius red staining. We found that the repaired tissues were mainly composed of thick type I collagen fibers in both the defect control group and polypropylene patch group, with a large amount of type III collagen fibers in the collagen group. The collagen structure of the CBD-bFGF group was disordered with both type I and type III collagen fibers (Fig. 4c).

Next, to determine the muscle regeneration, we performed α-actin staining. Results have shown a significant a-actin staining in the sham and collagen groups, but few positive signals in the polypropylene patch group and CBD-bFGF group

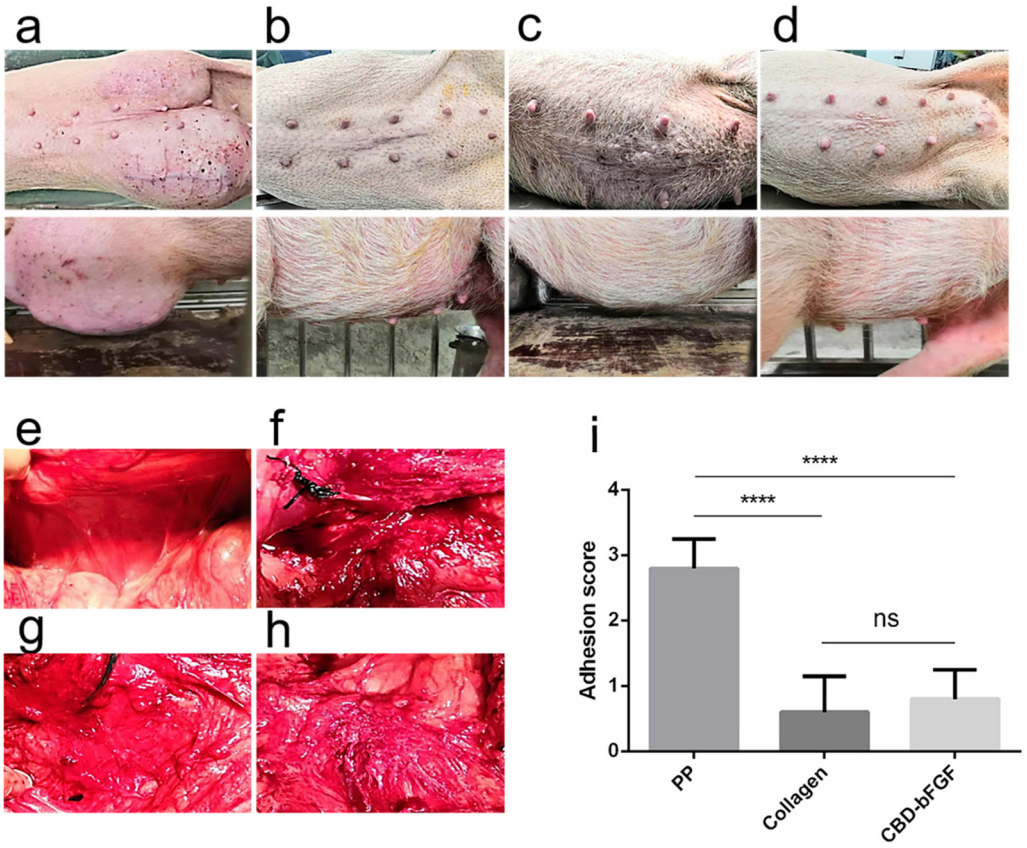

Fig. 3 General evaluation of repairing effect of the abdominal wall defect. (a–d) Gross abdominal appearance at 90 d after surgery. (a) Defect control group. (b) Polypropylene patch group. (c) Collagen group. (d) CBD-bFGF group. (e–i) Evaluation of adhesions between the organs in abdominal cavity and the implants at 90 d after surgery. (e) Normal muscles. (f) Polypropylene patch group. (g) Collagen group. (h) CBD-bFGF group. (i) The statistical analysis of the scores of adhesion. Data are presented as mean ± SD. ****$p < 0.01$.

(Fig. 5a–c). This further confirmed that the collagen biomaterials could induce muscle regeneration in abdominal hernia.

Previous studies have indicated that inflammation could inhibit the regeneration repair.[37,38] Thus, we detected the inflammatory response in different groups by staining CD163. At 90 d and 180 d after surgery, the CD163 positive areas were significantly higher in the polypropylene patch group than in the other groups (Fig. 5d–f). And there was no difference between the CBD-bFGF group and collagen group. These results indicated that the collagen based materials showed a relatively low inflammatory response than that of polypropylene.

3.4 Multiphoton microscopic imaging of repaired tissue

To further investigate the possible mechanism of collagen biomaterials inducing muscle regeneration, we tested the morphology and structure of the injured tissues. Multi-photon microimaging was performed on the repaired tissue 90 d after surgery, and Fig. 6a–e display the typical TPEF, SHG, and overlaid images and the corresponding HE-stained images of the repaired tissue, respectively. As can be seen in Fig. 6a, the muscle was characterized by muscle segment structures (arrow in Fig. 6a) and the collagen fibers surrounding them in the sham-operated group. However, only a large amount of collagen rather than muscle segment structures was found in the repair tissues of the defect control group (Fig. 6b), the polypropylene patch group (Fig. 6c) and the CBD-bFGF group (Fig. 6e). Although the repair tissue of the collagen group was also filled with collagen, muscle formation was found in multiple regions, which was completely different to the results of other groups. Surprisingly, the magnified images of some filled collagen in the collagen group displayed a collagen-conjoined muscle segment structure (arrow in Fig. 6d), indicating that the formation of muscle segments may be related to collagen.

3.5 Collagen patches induce a special collagen morphology and structure in the muscle regeneration processes

To understand the association between the change in collagen morphology and the regeneration of muscle segments more deeply, we selected five collagen regions at the muscle segment regeneration (arrow in Fig. 7a) front for quantitative analysis in the collagen group (Fig. 7a) and randomly selected five collagen regions at the repaired tissue for comparison in the defect control group (Fig. 7b), polypropylene patch group (Fig. 7c), and CBD-bFGF group (Fig. 7d). Fig. 7e–l reveal the

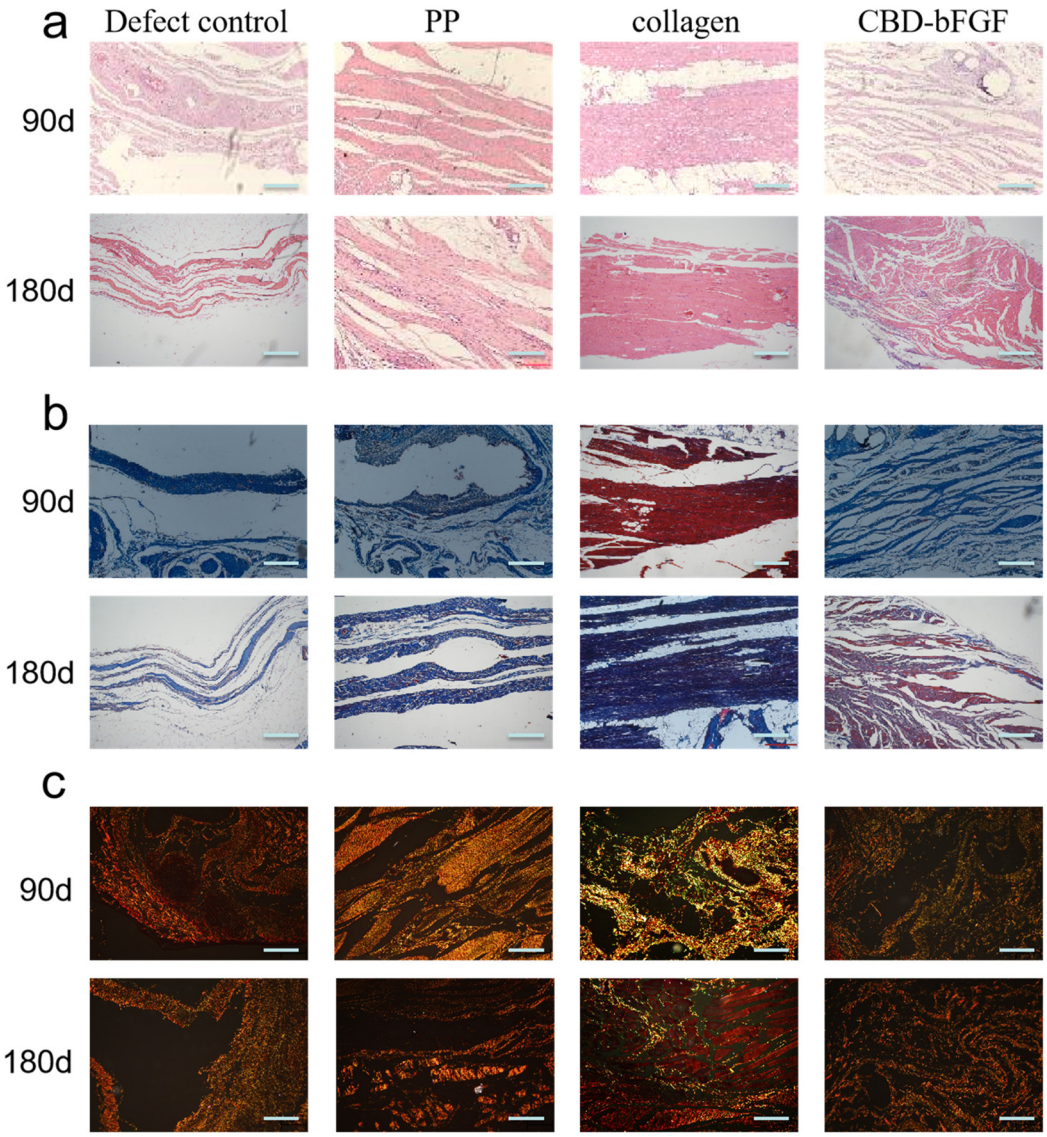

Fig. 4 Histological evaluation of the repair site by HE (a), Masson (b) and Sirus red stain (c) staining at 90 d and 180 d after surgery. Scale bars, 200 μm (a and b) or 500 μm (c).

quantitative characterization of collagen fiber among different groups. The collagen proportionate area and the fiber number were two features of the collagen content. They were 16.3% and 0.0010 ± 0.0004 μm^{-2} in the collagen group, respectively, which were significantly less than those in the defect control group (42.6% and 0.0026 ± 0.0005 μm^{-2}) and CBD-bFGF group (31% and 0.0019 ± 0.0007 μm^{-2}), but only showed a trend of being lower than that in the polypropylene patch group (21.8% and 0.0015 ± 0.0004 μm^{-2}) (Fig. 7e and f).

Similarly, the collagen fiber length and the collagen fiber width in the collagen group were significantly smaller than those in the defect control group and CBD-bFGF group, but only showed a trend of being lower than that in the polypropylene patch group (Fig. 7g and h). Their values were 25.048 ± 3.860 and 2.548 ± 0.463 μm, respectively, in the collagen group, 34.098 ± 3.574 and 3.669 ± 0.438 μm, respectively, in the defect control group, 27.437 ± 0.977 and 2.743 ± 0.226 μm, respectively, in the polypropylene patch group and 28.383 ± 5.711 and 3.042 ± 0.706 μm, respectively, in the CBD-bFGF group.

It is not surprising that the collagen fiber straightness at the muscle segment regeneration front in the collagen group (0.920 ± 0.006) was significantly higher than that in the defect control group (0.911 ± 0.005), the polypropylene patch group (0.905 ± 0.006) and the CBD-bFGF group (0.912 ± 0.011), which was consistent with the low level of collagen content, fiber length, and fiber width (Fig. 7i).

As one of the characteristic indicators of collagen densification, the collagen fiber cross-link density in the collagen group (1.31%) was significantly lower than that in the defect control group (1.63%) and the polypropylene patch group (1.9%), while it was only slightly lower than that in the

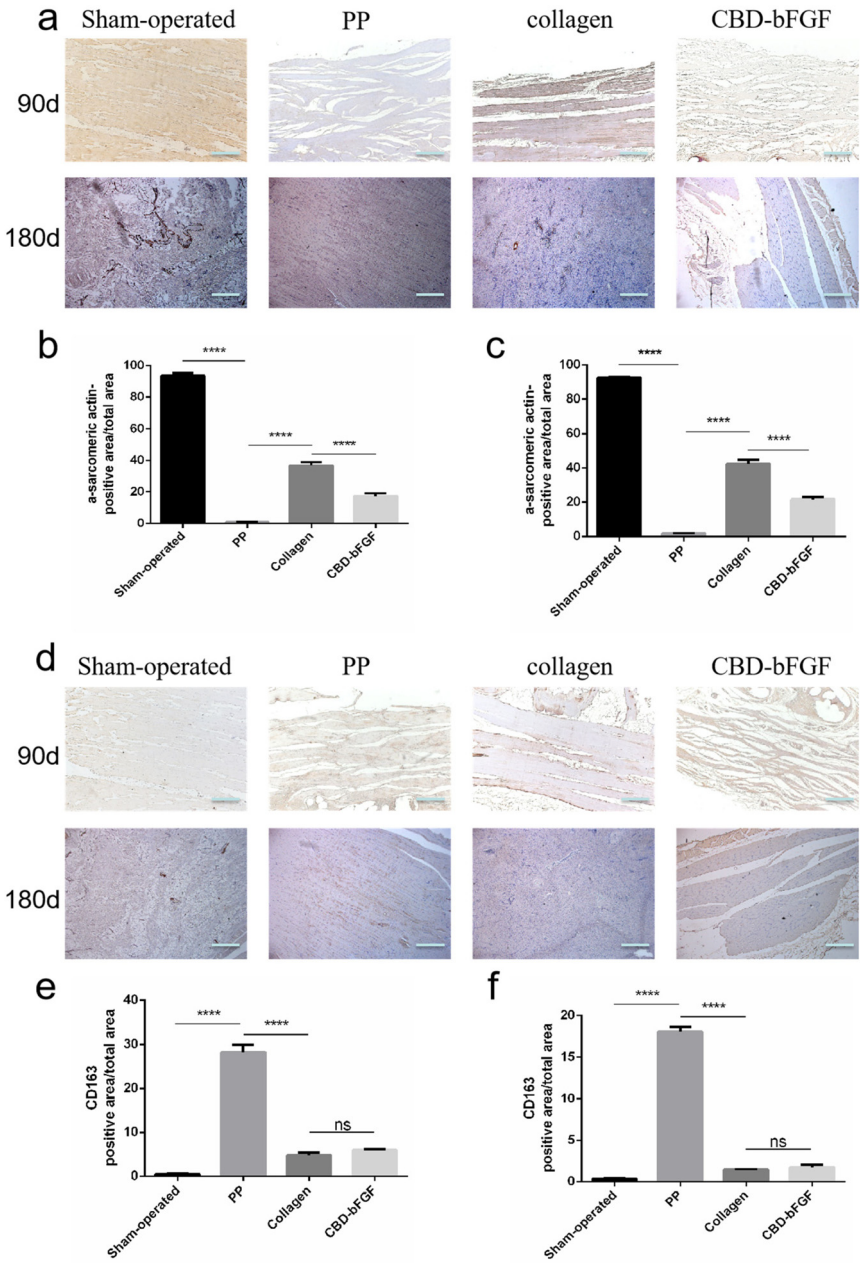

Fig. 5 Evaluation of abdominal wall muscle regeneration and inflammatory response. (a) Immunohistological staining of α-SMA, scale bars, 200 μm. (b) The statistical analysis of the percentage of a-sarcomeric actin positive area in implanted biomaterial at 90 days after surgery. (c) The statistical analysis of the percentage of a-sarcomeric actin positive area in implanted biomaterial at 180 days after surgery. (d) Immunohistological staining of CD163, scale bars, 200 μm. (e) The statistical analysis of the percentage of CD163 positive area in implanted biomaterial at 90 days after surgery. (f) The statistical analysis of the percentage of CD163 positive area in implanted biomaterial at 180 days after surgery. Data are presented as mean ± SD. ****$p < 0.01$.

CBD-bFGF group (1.58%) (Fig. 7j). In addition, there was no significant difference in the average cross-link space and orientation among the collagen group (22.868 ± 14.078 and 0.718, respectively), the defect control group (20.326 ± 0.796 and 0.854, respectively), the polypropylene patch group (17.090 ± 0.768 and 0.781, respectively) and the CBD-bFGF group (19.572 ± 2.094 and 0.777, respectively) (Fig. 7k and l).

In sum, quantitative analysis revealed that compared with the other groups, the microenvironment at the muscle segment regeneration front in the collagen group exhibited a significantly low-level or low-level trend in collagen percentage area, fiber number, length, width, and cross-link density, while exhibiting a significantly high-level in fiber straightness, suggesting that the massive generation and densification of collagen fibers may not be conducive to muscle regeneration.

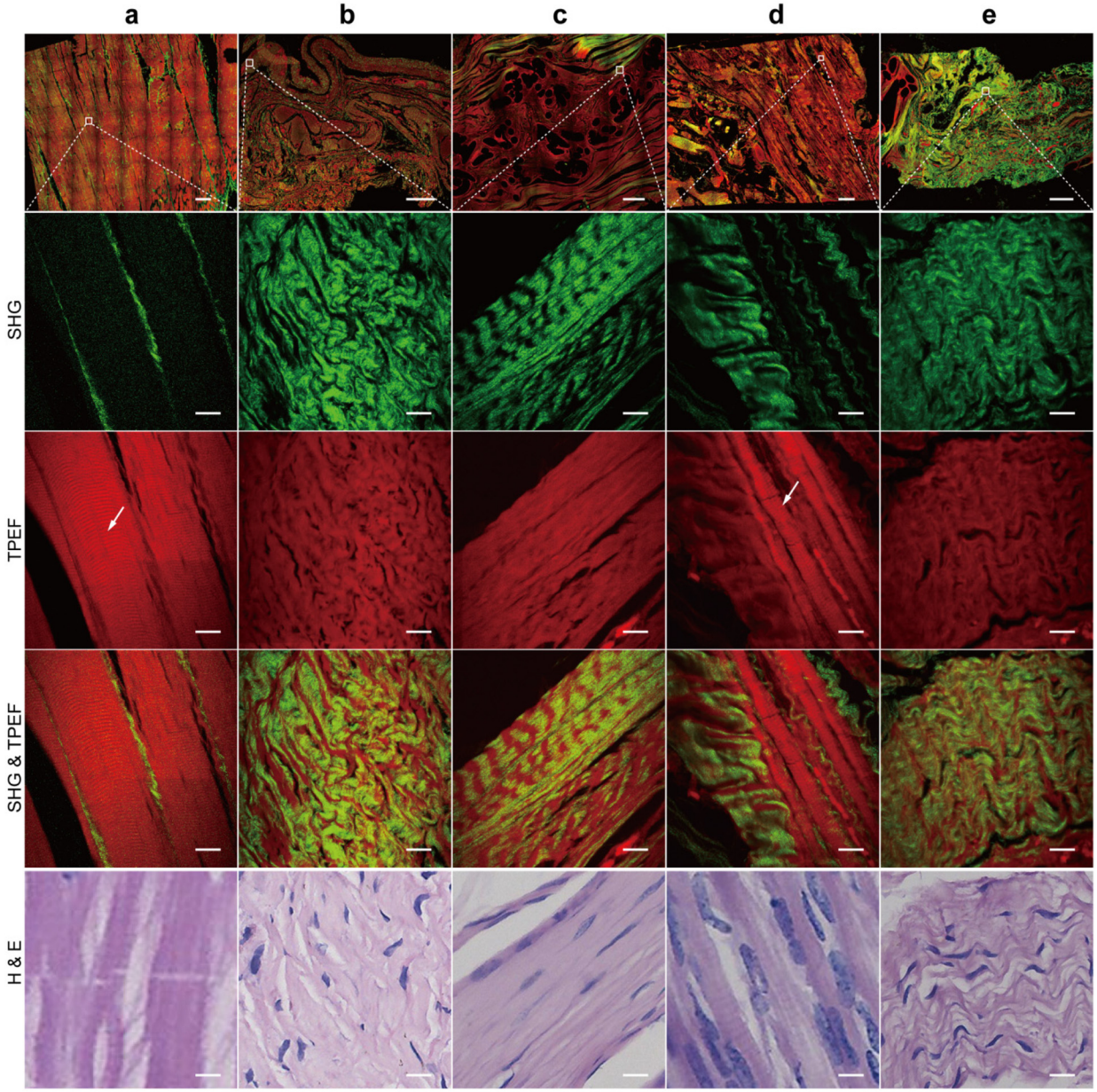

Fig. 6 The representative MPM imaging and the corresponding H&E-stained images of repair tissue. SHG images showed the morphology of collagen (colour-coded green). TPEF images showed the morphology of tissue cells and elastic fibers (colour-coded red). Overlay of the TPEF and SHG images allowed simultaneous localization of tissue cells and collagen. H&E-stained images confirmed muscle regeneration. (a) Sham-operated – group. (b) Defect control group. (c) Polypropylene patch group. (d) Collagen group. (e) CBD – bFGF group. Scale bar: 500 μm (1st row) or 50 μm (2nd to 5th rows). Arrows indicated muscle regeneration.

4. Discussion

The abdominal wall defect resulting from extensive resection or trauma belongs to VML, which seriously affects the life quality of the patients. However, it failed to reconstruct the abdominal wall as in a normal repair processes.[39] At present, the effective treatment is to use substitute materials to repair defective tissues. Synthetic materials, such as polypropylene and polytetrafluoroethylene, are the main clinical patch materials.[30] However, these materials could not induce the regeneration of the muscle tissues, and moreover lead to frequent complications due to non-degradation and immune rejection.[40]

Therefore, it is urgently needed to develop biodegradable materials to induce the regenerative repair of abdominal wall defects. Recently, some kinds of materials that might fit this demand include naturally derived materials (*e.g.*, collagen, keratin, and alginate), cell-free tissue substrates (*e.g.*, acellular tissues from the bladder or small intestine), synthetic polymers (*e.g.*, polyglycolic acid [PGA], polylactic acid [PLA], and

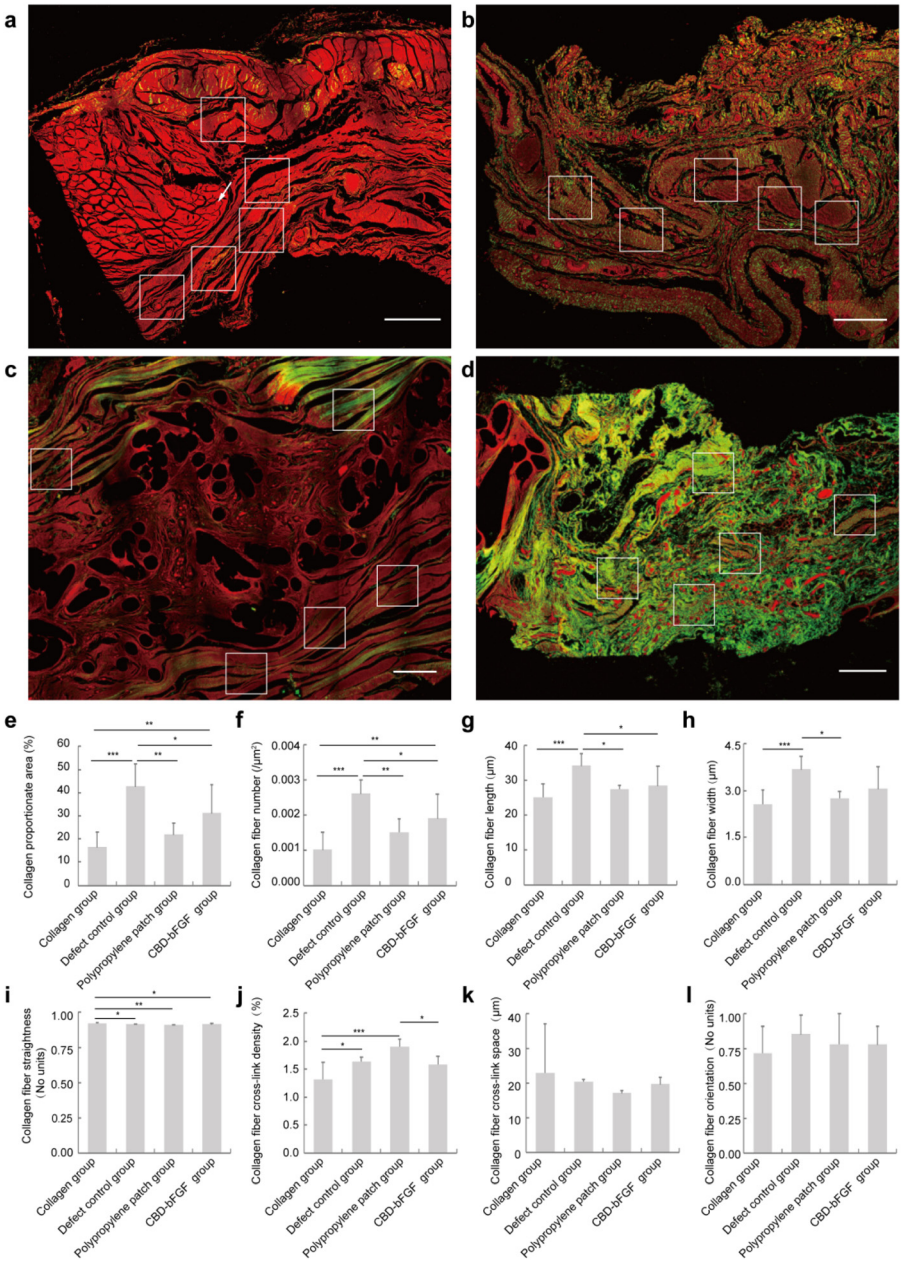

Fig. 7 The collagen morphology and structure of the repaired tissues was analysed by MPM. The collagen was colour-coded green, while tissue cells and elastic fibers were colour-coded red. (a) Collagen group. (b) Defect control group. (c) Polypropylene patch group. (d) CBD-bFGF group. (e) Quantitative results of collagen percentage area. (f) Quantitative results of collagen fiber number. (g) Quantitative results of collagen fiber length. (h) Quantitative results of collagen fiber width. (i) Quantitative results of collagen fiber straightness. (j) Quantitative results of collagen fiber cross-link density. (k) Quantitative results of collagen fiber cross-link space. (l) Quantitative results of collagen fiber orientation. Scale bar: 500 μm. The quantitative results are presented as mean ± SD. *$P < 0.05$, **$P < 0.01$, ***$P < 0.001$. The Arrow indicated muscle regeneration.

polylactic acid – glycolic acid [PLGA]), *etc.*[41–45] In this study, we used a biological collagen scaffold prepared from fresh bovine aponeurosis. After acellular treatment, type I collagen was well preserved. Compared with synthetic or biopolymer scaffolds, this kind of material is more advantageous in biocompatibility and a natural extracellular matrix structure. At the same time, we fused a collagen-binding peptide (TKKTLRT) with bFGF to synthesize CBD-bFGF, which can specifically bind to biological collagen scaffolds. In previous studies, we have proved that such biomaterials, especially CBD-bFGF, can promote the repair of abdominal wall muscle defects in rats.[27] However, there is still a lack of evidence for abdominal wall defects in large animals. Therefore, in this study, we evaluated the effects of a biological collagen scaffold and a CBD-bFGF collagen scaffold on the repair of abdominal wall defects in Bama miniature pigs, and compared these with the traditional polypropylene patches.

Recurrence and adhesion are the main indexes to evaluate the structural recovery of the abdominal wall, which usually causes intestinal obstruction, chronic pain, and even infertility.[46] Our results showed that both collagen materials and polypropylene patches can effectively repair a defect and prevent the recurrence of abdominal hernia. However, the adhesion of biological collagen materials with or without growth factors was significantly less than that of the polypropylene patch group. Inflammation is one of the main causes of adhesion formation during abdominal wall repair. Due to surgical trauma and a foreign body reaction, plasminogen activators are inhibited, which directly increased the deposition of fibrin matrix to form an organized fibrous adhesion.[47,48] It is necessary to reduce inflammation to prevent the formation of adhesions. Biological collagen materials have low antigenicity and inflammation and have been used in Clinical haemostasis.[23] In this study, we also evaluated the inflammatory response of the repaired tissues with anti-CD163 antibody, and the results showed that the inflammatory response of the collagen biomaterials group with and without modified CBD-bFGF was minimal compared with that of the polypropylene patch group, which was consistent with the results of the adhesion evaluation.

More importantly, we evaluated the muscle repair of the most important defect tissue, and found that no matter 90 d or 180 d after surgery, the use of biological collagen scaffolds could regenerate muscle fiber structures similar to those of natural muscles. Different from the previously observed repair effect of abdominal wall defects in rats, the muscle fibers in the collagen group were arranged neatly, similar to those in the sham operated-group, which was significantly better than that of the CBD-bFGF group. α-Actin staining also confirmed the results. Instead of muscle regeneration, the repair tissues in the CBD-bFGF group and polypropylene group were composed mainly of collagen fibers. Our work presents the first evidence that collagen membrane material could induce muscle regeneration in large animals, which promises its clinical transformation potential.

To further detect the possible mechanism of the regeneration induced by collagen materials, we constructed MPM technology to evaluate the effect of tissue repair. This is an advanced medical imaging technology based on nonlinear optical effects such as multi-photon excited fluorescence and harmonic generation caused by the interaction between the laser and biological tissue. It has the advantages of a high sensitivity and high spatial resolution imaging of tissue microstructure and a low lethality to biological tissue. On the one hand, it displays the structure of cells by capturing the TPEF signal (red in the MPM image) generated by intrinsic fluorophores in cells, and on the other hand, it displays the morphology of collagen fibers *in situ* by capturing the SHG signal (green in the MPM image) generated by non-centrosymmetric structural molecules such as collagen. Through this simple colour difference and switching or overlapping of two signal channels (TPEF signal and SHG signal), MPM can identify the morphology and position of collagen fibers in unstained tissue, which is the biggest advantage of MPM. Combined with a self-developed image-processing algorithm, the eight collagen morphological features of repair tissue are accurately quantified to preliminarily analyse changes in the microenvironment of muscle regeneration. The results showed that the collagen morphology and structure of the repaired tissues in the collagen group were different from those in the other groups, with lower levels of collagen content, and shorter, thinner, and straighter collagen fibers. The microenvironment at the muscle segment regeneration front in the collagen group was more sparse than that in other groups, which left room for further extension of the regenerated muscle. However, the underlying mechanism still needs further study to make sure of the factors causing the environment at the muscle segment regeneration front in the collagen group to be looser than that in other repair groups, as well as the collagen-conjoined muscle segment structure in the collagen group.

The strength of biomaterials is the major limiting factor in the clinical use of abdominal wall reconstruction. In this study, the tensile strength of the collagen membrane was measured at 24.53 MPa. The tearing force was measured at 16.82 N, which, although lower than that of normal tissue, remains suitable for withstanding abdominal pressure in large animals. However, it should be noted that the collagen barrier may expand in the humid environment of the abdomen, leading to deformation of the membrane material.[49] Excessive expansion can significantly affect the sustained repair effect of the implanted material.[50,51] In order to evaluate the efficacy of abdominal wall reconstruction in the early stages, the research group measured the tensile strength of the implanted biomaterial on the 90th day following abdominal wall defect in rats. The average ultimate tensile strength of the simple collagen membrane was determined to be 7.07 ± 2.47 N.[27] Moreover, upon harvesting the repaired tissue of Bama pigs on the 90th day, the residual collagen materials were scarce, indicating variations in the degree of collagen absorption among different species. Next, monitoring changes in implant strength over time will be conducted to further optimize the material's resistance to deformation.

In addition, in both the Bama miniature pig model and the rat model, the dosage of CBD-bFGF used was consistent, with both weighing 64 μg per collagen membrane. Similarly, in the urethral cavernosum repair model and bladder reconstruction model, the CBD-bFGF dose of collagen scaffold was also 64 μg g^{-1} collagen membrane weight.[52,53] Previous experience suggests that at this dose, the N-terminal of bFGF can bind to the specific collagen binding domain to the greatest extent without affecting the factor activity.[28] High dose of bFGF, on the other hand, may lead to excessive fibroblast proliferation of and massive secretion of extracellular matrix. Lu J., *et al.* found that excessive bFGF can cause tendon adhesion and scar tissue formation.[54] Moreover, high doses of bFGF have been associated with thrombocytopenia, nephrotoxicity, and even the activation of some malignant cells.[55,56] In the present study, the current dosage of CBD-bFGF induced massive secretion of the extracellular matrix. Therefore, we propose

that a much higher dose of CBD-bFGF would aggravate local fibrosis while inducing regenerative repair. However, further investigation is required to elucidate the mechanism underlying CBD-bFGF-induced regenerative repair in rat models and fibrotic repair in Bama miniature pig models.

5. Conclusions

Our results show a low probability of recurrence, low degree of adhesion and mild local inflammatory reaction in the repaired abdominal hernia by biomaterials in Bama miniature pigs. The biological collagen scaffold can effectively reduce the fibrosis in the repaired tissue and induce the regenerative repair of abdominal muscle. Therefore, this biomaterial shows its potential for clinical application as a countermeasure to VML after abdominal wall defects.

Author contributions

Conceptualization: Chunmeng Shi, Jianwu Dai and Jianxin Chen; methodology: Langfan Qu, Zelin Chen, Jianhua Chen and Yibo Gan; validation: Chunmeng Shi, Jianxin Chen and Jianwu Dai; formal analysis: Langfan Qu, Zelin Chen, Jianhua Chen and Yibo Gan; investigation: Langfan Qu, Zelin Chen, Yibo Gan, Xu Tan, Yu Wang and Can Zhang; software: Langfan Qu and Jianhua Chen; resources: Langfan Qu, Zelin Chen, Yibo Gan and Bing Chen; data curation: Langfan Qu, Zelin Chen and Jianhua Chen; visualization: Langfan Qu and Jianhua Chen; supervision: Chunmeng Shi, Jianwu Dai and Jianxin; project administration: Chunmeng Shi; funding acquisition: Chunmeng Shi; writing-original draft: Langfan Qu, Zelin Chen and Jianhua Chen; writing-review & editing: Chunmeng Shi and Jianxin Chen.

Conflicts of interest

The authors declare that they have no competing financial interests.

Acknowledgements

This work was supported by National Key Research and Development Program of China (2016YFC1000805).

References

1 R. Langer and J. P. Vacanti, *Science*, 1993, **260**, 920–926.
2 B. J. Kwee and D. J. Mooney, *Curr. Opin. Biotechnol*, 2017, **47**, 16–22.
3 T. H. Qazi, D. J. Mooney, M. Pumberger, S. Geissler and G. N. Duda, *Biomaterials*, 2015, **53**, 502–521.
4 A. S. Brack and T. A. Rando, *Cell Stem Cell*, 2012, **10**, 504–514.
5 F. Relaix and P. S. Zammit, *Development*, 2012, **139**, 2845–2856.
6 N. J. Turner and S. F. Badylak, *Cell Tissue Res.*, 2012, **347**, 759–774.
7 B. F. Grogan and J. R. Hsu, *J. Am. Acad. Orthop. Surg.*, 2011, **19**(Suppl 1), S35–S37.
8 J. Ma, S. Sahoo, A. R. Baker and K. A. Derwin, *J. Biomed. Mater. Res., Part B*, 2015, **103**, 355–364.
9 O. Guillaume, A. H. Teuschl, S. Gruber-Blum, R. H. Fortelny, H. Redl and A. Petter-Puchner, *Adv. Healthc. Mater.*, 2015, **4**, 1763–1789.
10 S. F. Badylak, *Semin. Cell Dev. Biol.*, 2002, **13**, 377–383.
11 I. Eugenis, D. Wu and T. A. Rando, *Biomaterials*, 2021, **278**, 121173.
12 K. Sadtler, K. Estrellas, B. W. Allen, M. T. Wolf, H. Fan, A. J. Tam, C. H. Patel, B. S. Luber, H. Wang, K. R. Wagner, J. D. Powell, F. Housseau, D. M. Pardoll and J. H. Elisseeff, *Science*, 2016, **352**, 366–370.
13 B. N. Brown, R. Londono, S. Tottey, L. Zhang, K. A. Kukla, M. T. Wolf, K. A. Daly, J. E. Reing and S. F. Badylak, *Acta Biomater.*, 2012, **8**, 978–987.
14 J. M. Fishman, M. W. Lowdell, L. Urbani, T. Ansari, A. J. Burns, M. Turmaine, J. North, P. Sibbons, A. M. Seifalian, K. J. Wood, M. A. Birchall and P. De Coppi, *Proc. Natl. Acad. Sci. U. S. A.*, 2013, **110**, 14360–14365.
15 A. Aurora, J. L. Roe, B. T. Corona and T. J. Walters, *Biomaterials*, 2015, **67**, 393–407.
16 B. M. Sicari, J. P. Rubin, C. L. Dearth, M. T. Wolf, F. Ambrosio, M. Boninger, N. J. Turner, D. J. Weber, T. W. Simpson, A. Wyse, E. H. Brown, J. L. Dziki, L. E. Fisher, S. Brown and S. F. Badylak, *Sci. Transl. Med.*, 2014, **6**, 234ra258.
17 B. T. Corona, X. Wu, C. L. Ward, J. S. McDaniel, C. R. Rathbone and T. J. Walters, *Biomaterials*, 2013, **34**, 3324–3335.
18 N. J. Turner, J. S. Badylak, D. J. Weber and S. F. Badylak, *J. Surg. Res.*, 2012, **176**, 490–502.
19 J. E. Valentin, N. J. Turner, T. W. Gilbert and S. F. Badylak, *Biomaterials*, 2010, **31**, 7475–7484.
20 K. Garg, C. L. Ward and B. T. Corona, *Inflammation Cell Signaling*, 2014, **1**, e530.
21 C. L. Dearth, T. J. Keane, C. A. Carruthers, J. E. Reing, L. Huleihel, C. A. Ranallo, E. W. Kollar and S. F. Badylak, *Acta Biomater.*, 2016, **33**, 78–87.
22 S. Ogawa, M. Tomita, K. Shimizu and K. Yoshizato, *J. Biotechnol.*, 2007, **128**, 531–544.
23 L. Kolácná, J. Bakesová, F. Varga, E. Kostáková, L. Plánka, A. Necas, D. Lukás, E. Amler and V. Pelouch, *Physiol. Res.*, 2007, **56**(Suppl 1), S51–S60.
24 S. Nakamura, M. Nambu, T. Ishizuka, H. Hattori, Y. Kanatani, B. Takase, S. Kishimoto, Y. Amano, H. Aoki, T. Kiyosawa, M. Ishihara and T. Maehara, *J. Biomed. Mater. Res., Part A*, 2008, **85**, 619–627.

25 M. Fujita, M. Ishihara, M. Simizu, K. Obara, T. Ishizuka, Y. Saito, H. Yura, Y. Morimoto, B. Takase, T. Matsui, M. Kikuchi and T. Maehara, *Biomaterials*, 2004, **25**, 699–706.
26 I. G. Kim, S. H. Oh, J. Y. Lee, J. Y. Lee and J. H. Lee, *Tissue Eng., Part A*, 2011, **17**, 1527–1535.
27 C. Shi, W. Chen, Y. Zhao, B. Chen, Z. Xiao, Z. Wei, X. Hou, J. Tang, Z. Wang and J. Dai, *Biomaterials*, 2011, **32**, 753–759.
28 W. Zhao, B. Chen, X. Li, H. Lin, W. Sun, Y. Zhao, B. Wang, Y. Zhao, Q. Han and J. Dai, *J. Biomed. Mater. Res., Part A*, 2007, **82**, 630–636.
29 X. Li, H. Sun, N. Lin, X. Hou, J. Wang, B. Zhou, P. Xu, Z. Xiao, B. Chen, J. Dai and Y. Hu, *Biomaterials*, 2011, **32**, 8172–8181.
30 J. M. Bellón, M. Rodríguez, N. García-Honduvilla, V. Gómez-Gil, G. Pascual and J. Buján, *J. Biomed. Mater. Res., Part B*, 2009, **89**, 448–455.
31 P. Losi, A. Munaò, D. Spiller, E. Briganti, I. Martinelli, M. Scoccianti and G. Soldani, *J. Mater. Sci. Mater. Med.*, 2007, **18**, 1939–1944.
32 A. S. Gobin, C. E. Butler and A. B. Mathur, *Tissue Eng.*, 2006, **12**, 3383–3394.
33 D. Wanduku, *Heliyon*, 2022, **8**, e12622.
34 A. M. Stein, D. A. Vader, L. M. Jawerth, D. A. Weitz and L. M. Sander, *J. Microsc.*, 2008, **232**, 463–475.
35 S. Xu, C. H. Kang, X. Gou, Q. Peng, J. Yan, S. Zhuo, C. L. Cheng, Y. He, Y. Kang, W. Xia, P. T. So, R. Welsch, J. C. Rajapakse and H. Yu, *J. Biophotonics*, 2016, **9**, 351–363.
36 K. E. Frisch, S. E. Duenwald-Kuehl, H. Kobayashi, C. S. Chamberlain, R. S. Lakes and R. Vanderby Jr., *Acta Histochem.*, 2012, **114**, 140–144.
37 V. Moiseeva, A. Cisneros, V. Sica, O. Deryagin, Y. Lai, S. Jung, E. Andrés, J. An, J. Segalés, L. Ortet, V. Lukesova, G. Volpe, A. Benguria, A. Dopazo, S. A. Benitah, Y. Urano, A. Del Sol, M. A. Esteban, Y. Ohkawa, A. L. Serrano, E. Perdiguero and P. Muñoz-Cánoves, *Nature*, 2023, **613**, 169–178.
38 K. L. McKinley, M. T. Longaker and S. Naik, *Science*, 2023, **380**, 796–798.
39 P. De Coppi, S. Bellini, M. T. Conconi, M. Sabatti, E. Simonato, P. G. Gamba, G. G. Nussdorfer and P. P. Parnigotto, *Tissue Eng.*, 2006, **12**, 1929–1936.
40 H. Hjort, T. Mathisen, A. Alves, G. Clermont and J. P. Boutrand, *Hernia*, 2012, **16**, 191–197.
41 G. Pascual, S. Sotomayor, M. Rodríguez, B. Pérez-Köhler and J. M. Bellón, *PLoS One*, 2012, **7**, e52628.
42 C. R. Deeken, B. J. Eliason, M. D. Pichert, S. A. Grant, M. M. Frisella and B. D. Matthews, *Ann. Surg.*, 2012, **255**, 595–604.
43 C. F. Bellows, A. Smith, J. Malsbury and W. S. Helton, *Am. J. Surg.*, 2013, **205**, 85–101.
44 E. Peeters, K. W. van Barneveld, M. H. Schreinemacher, G. De Hertogh, Y. Ozog, N. Bouvy and M. Miserez, *J. Surg. Res.*, 2013, **180**, 274–283.
45 G. Pascual, B. Pérez-Köhler, M. Rodríguez, S. Sotomayor and J. M. Bellón, *Surg. Endosc.*, 2014, **28**, 559–569.
46 H. Ellis, B. J. Moran, J. N. Thompson, M. C. Parker, M. S. Wilson, D. Menzies, A. McGuire, A. M. Lower, R. J. Hawthorn, F. O'Brien, S. Buchan and A. M. Crowe, *Lancet*, 1999, **353**, 1476–1480.
47 N. Wasserberg, J. W. Nunoo-Mensah, P. Ruiz and A. G. Tzakis, *J. Surg. Res.*, 2007, **141**, 294–298.
48 M. van 't Riet, P. J. de Vos van Steenwijk, F. Bonthuis, R. L. Marquet, E. W. Steyerberg, J. Jeekel and H. J. Bonjer, *Ann. Surg.*, 2003, **237**, 123–128.
49 J. W. Burger, J. A. Halm, A. R. Wijsmuller, S. ten Raa and J. Jeekel, *Surg. Endosc.*, 2006, **20**, 1320–1325.
50 S. J. Wu, H. Yuk, J. Wu, C. S. Nabzdyk and X. Zhao, *Adv. Mater.*, 2021, **33**, e2007667.
51 H. Yuk, C. E. Varela, C. S. Nabzdyk, X. Mao, R. F. Padera, E. T. Roche and X. Zhao, *Nature*, 2019, **575**, 169–174.
52 H. Tang, W. Jia, X. Hou, Y. Zhao, Y. Huan, W. Chen, W. Yu, M. M. Ou Zhu, G. Ye, B. Chen and J. Dai, *Biomed. Mater.*, 2018, **13**, 031001.
53 C. Shi, W. Chen, B. Chen, T. Shan, W. Jia, X. Hou, L. Li, G. Ye and J. Dai, *Biomater. Sci.*, 2017, **5**, 2427–2436.
54 J. Lu, L. Jiang, Y. Chen, K. Lyu, B. Zhu, Y. Li, X. Liu, X. Liu, L. Long, X. Wang, H. Xu, D. Wang and S. Li, *Front. Physiol.*, 2022, **13**, 852795.
55 E. F. Unger, L. Goncalves, S. E. Epstein, E. Y. Chew, C. B. Trapnell, R. O. Cannon 3rd and A. A. Quyyumi, *Am. J. Cardiol.*, 2000, **85**, 1414–1419.
56 S. E. Epstein, S. Fuchs, Y. F. Zhou, R. Baffour and R. Kornowski, *Cardiovasc. Res.*, 2001, **49**, 532–542.